



HAL
open science

Increasing the π -Expansive Ligands in Ruthenium(II) Polypyridyl Complexes: Synthesis, Characterization, and Biological Evaluation for Photodynamic Therapy Applications

Maria Dalla Pozza, Pierre Mesdom, Ahmad Abdullrahman, Tayler Prieto Otoy, Philippe Arnoux, Céline Frochot, Germain Niogret, Bruno Saubaméa, Pierre Burckel, James P Hall, et al.

► **To cite this version:**

Maria Dalla Pozza, Pierre Mesdom, Ahmad Abdullrahman, Tayler Prieto Otoy, Philippe Arnoux, et al.. Increasing the π -Expansive Ligands in Ruthenium(II) Polypyridyl Complexes: Synthesis, Characterization, and Biological Evaluation for Photodynamic Therapy Applications. *Inorganic Chemistry*, 2023, 62 (45), pp.18510-18523. 10.1021/acs.inorgchem.3c02606 . hal-04269310

HAL Id: hal-04269310

<https://hal.science/hal-04269310>

Submitted on 3 Nov 2023

HAL is a multi-disciplinary open access archive for the deposit and dissemination of scientific research documents, whether they are published or not. The documents may come from teaching and research institutions in France or abroad, or from public or private research centers.

L'archive ouverte pluridisciplinaire **HAL**, est destinée au dépôt et à la diffusion de documents scientifiques de niveau recherche, publiés ou non, émanant des établissements d'enseignement et de recherche français ou étrangers, des laboratoires publics ou privés.



Distributed under a Creative Commons Attribution - NonCommercial 4.0 International License

Increasing the π -expansive ligands in Ruthenium(II) polypyridyl complexes: synthesis, characterisation and biological evaluation for photodynamic therapy applications

Maria Dalla Pozza,^a Pierre Mesdom,^a Ahmad Abdullrahman,^b Tayler D. Prieto Otoy,^c Philippe Arnoux,^d Céline Frochot,^d Germain Niogret,^e Bruno Saubaméa,^f Pierre Burckel,^g James P. Hall,^b Marcel Hollenstein,^e Christine J. Cardin,^c and Gilles Gasser^{a*}

^a Chimie ParisTech, PSL University, CNRS, Institute of Chemistry for Life and Health, Paris, 75005 France.

^b Department of Pharmacy, Chemistry and Pharmacy Building, University of Reading, Whiteknights Campus, Reading, Berkshire, RG6 6AD UK

^c Department of Chemistry, University of Reading, Whiteknights, Reading, RG6 6AD, UK.

^d Université de Lorraine, CNRS, LRGP, F-54000 Nancy, France.

^e Institut Pasteur, Université de Paris Cité, CNRS UMR3523, Département of Structural Biology and Chemistry, Laboratory for Bioorganic Chemistry of Nucleic Acids, Paris, 75015 France.

^f Université Paris Cité, INSERM, CNRS, P-MIM, Plateforme d'Imagerie Cellulaire et Moléculaire (PICMO), F-75006 Paris, France.

^g Université de Paris, Institut de physique du globe de Paris, CNRS, F-75005 Paris, France.

* Corresponding author: Email: gilles.gasser@chimieparistech.psl.eu; www: www.gassergroup.com

Keywords: Bioinorganic Chemistry; Cancer; Metals in Medicine; Photodynamic Therapy; Ru(II) polypyridyl compounds.

Abbreviations: PDT (Photodynamic Therapy), PS (Photosensitiser), DIP (4,7-diphenyl-1,10-phenanthroline), dppn (benzo[*i*]dipyrido[3,2-*a*:2',3'-*c*]phenazine), dppz (dipyrido[3,2-*a*:2',3'-*c*]phenazine), TAP (1,4,5,8-tetraazaphenanthrene), phen (1,10-phenanthroline), phendione (1,10-

Phenanthroline-5,6-dione), MLCT (Metal to Ligand Charge Transfer), DMSO (dimethylsulfoxide), CT26 (mouse colon carcinoma), HT29 (human colon adenocarcinoma), RPE-1 (eye pigmented retinal epithelium), PpIX (protoporphyrin IX), ICP-MS (inductively coupled plasma-mass-spectrometry), mtDNA (mitochondrial DNA), nDNA (nuclear DNA), FCCP (carbonyl cyanide 4-(trifluoromethoxy)phenylhydrazone), CD (circular dichroism), dsDNA (double stranded DNA), PI(Phototoxicity Index), OCR (Oxygen Consumption Rate).

Abstract

Lack of selectivity is one of the main issues with currently used chemotherapies, causing damage not only to altered cells, but also to healthy cells. Over the last decades, photodynamic therapy (PDT) has risen as a promising therapeutic tool due to its potential to treat diseases like cancer or bacterial infections with a high spatio-temporal control. Ruthenium(II) polypyridyl compounds are gaining attention for their application as photosensitisers (PS), since they are generally non-toxic in dark conditions, while they show remarkable toxicity after light irradiation. In this work, four Ru(II) polypyridyl compounds with sterically expansive ligands were studied as PDT agents. The Ru(II) complexes were synthesized using an alternative route to the ones described in the literature, which resulted for an improvement of the synthesis yields. Solid-state structures of compounds **[Ru(DIP)₂phen]Cl₂** and **[Ru(dppz)₂phen](PF₆)₂** have also been obtained. It is well known that the compound [Ru(dppz)(phen)₂]Cl₂ binds to DNA by intercalation. Therefore, we used **[Ru(dppz)₂phen]Cl₂** as a model for DNA interaction studies, showing that it stabilised two different sequences of duplex DNA. Most of the synthesized Ru(II) derivatives showed very promising singlet oxygen quantum yields, together with noteworthy photo-cytotoxic properties against two different cancer cell lines, with IC₅₀ in the micro- or even nanomolar range (0.06-7 μM). Confocal microscopy studies showed that **[Ru(DIP)₂phen]Cl₂** and **[Ru(DIP)₂TAP]Cl₂** accumulate preferentially in mitochondria, while no mitochondria internalisation was observed for the other compounds. Although **[Ru(dppn)₂phen](PF₆)₂** did not accumulate in mitochondria, it interestingly triggered an impairment in mitochondria respiration. Among others, **[Ru(dppn)₂phen](PF₆)₂** stands out for its very good IC₅₀ values, correlated with a very high singlet oxygen quantum yield and mitochondrial respiration disruption.

Introduction

Photodynamic Therapy (PDT) is a well-established medical technique used for the treatments of localised diseases, and is a valuable supplement or alternative to chemotherapy, radiotherapy or immunotherapy for the treatment of some forms of cancer. PDT was developed to decrease the well-known side-effects of chemotherapy, which very often lacks selectivity.¹ PDT is based on the use of light, a photosensitiser (PS) and oxygen. The PS is ideally non-toxic in dark conditions and becomes toxic once irradiated with light at a desired wavelength. After being excited with light at a specific wavelength, the PS* often undergoes intersystem crossing (ISC), leading to a triplet excited state T_1 . From this excited state, energy can be transferred to the surrounding biomolecules (PDT type I) or directly to molecular oxygen in its ground state (3O_2) (PDT type II) to produce reactive oxygen species (ROS), such as singlet oxygen (1O_2), superoxide radical ($O_2^{\cdot-}$), hydroxyl radical (HO^{\cdot}), and hydrogen peroxide (H_2O_2). An ideal PS is characterised by the ability to absorb light in the therapeutic window (600-900 nm), an appropriate energy of the triplet state, and a lifetime of the triplet state long enough to allow production of ROS. The most interesting feature of PDT is the spatio-temporal control of drug-activation, which makes it possible to have a specific target, decreasing the severe side effects caused by the diffusion of a toxic drug in the entire body.^{2,3}

Ruthenium(II) polypyridyl compounds have been widely studied in the last decades due to their promising photodynamic properties.⁴⁻¹¹ In fact, the possibility to tune the electronic configuration of the metal complexes by changing the ligands, their outstanding values of 1O_2 formation quantum yield after light activation, and their ability to interact with biological targets like DNA or proteins, make this class of compounds very versatile for different applications. Remarkably, by modulating the choice of the ligands, it is possible to obtain a red-shift in the absorption spectra, an increased cellular uptake, better targeting properties, and improved ROS production, responsible for cell death.¹²⁻¹⁴ In 2017, the Ru(II)-based compound TLD1433 designed by McFarland *et al.* entered clinical trials for bladder cancer, increasing the interest of this versatile class of compounds.^{15,16}

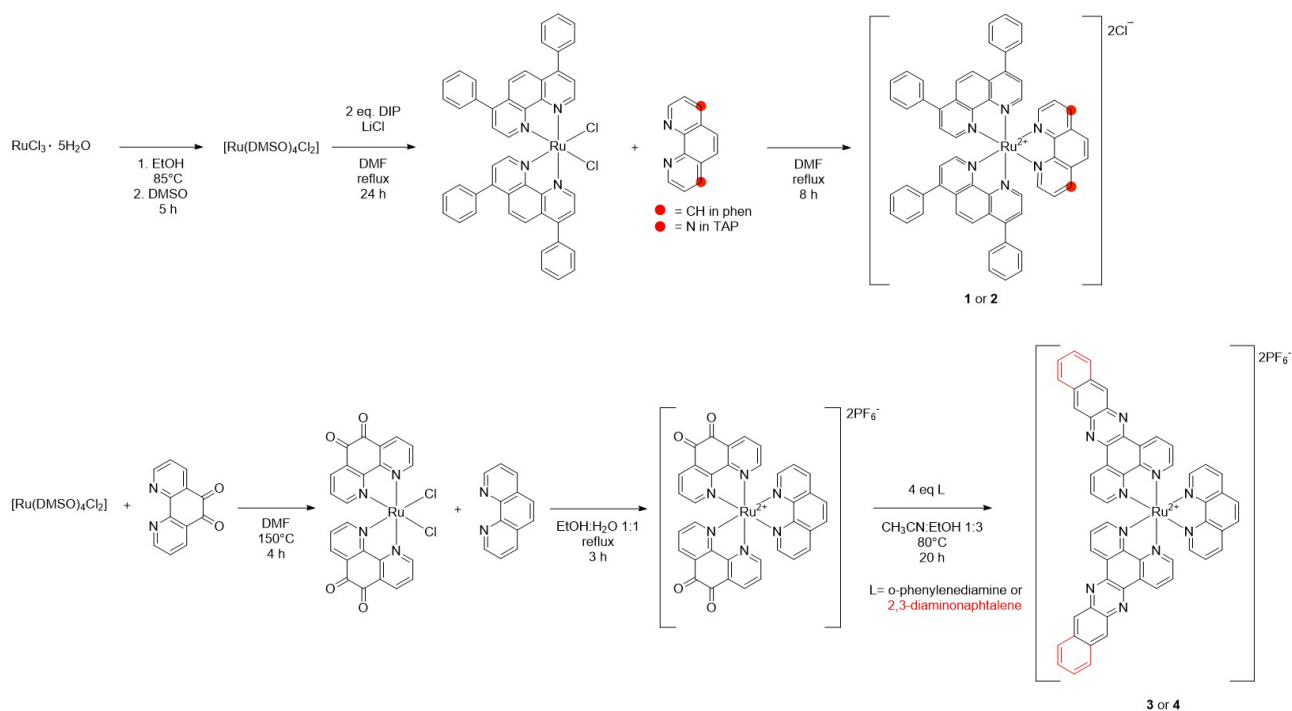
Heteroleptic Ru(II) compounds with one bulky intercalating ligand have largely been reported in the literature for their photodynamic and DNA intercalating properties.¹⁷⁻²⁰ The complex $[Ru(dppz)(phen)_2]Cl_2$ has been extensively studied by Barton *et al.* for its high binding affinity to DNA and its "light-switch" properties once intercalated into the double helix of DNA.^{18,19,21} Taking into account the need for increasing the affinity of Ru(II)-based PSs for biological targets and with the aim to improve the 1O_2 production of these compounds, in this work, we planned to design Ru(II) derivatives with additional π -extended ligands such as the benzo[i]dipyrido[3,2-a:2',3'-c]phenazine

correlated with very good $^1\text{O}_2$ quantum yields. Therefore, we went more in depth studying the internalisation of the most promising compounds in nuclei and mitochondria, and we checked their effect on the mitochondrial respiration.

Results and Discussion

Synthesis and characterisation

The Ru(II) derivatives were synthesized using different strategies. All of them were prepared starting from $[\text{Ru}(\text{DMSO})_4\text{Cl}_2]$, which has already been reported in the literature as a useful precursor for this kind of compounds.²⁶ The complexes bearing two DIP ligands, **1** and **2**, were obtained by coordination of the two DIP ligands with the metal centre in anhydrous DMF, followed by coordination with the phen or TAP ligand to obtain the final compound, after purification by silica column chromatography, with yields of 73% and 42%, respectively (**Scheme 1**). The synthesis of $[\text{Ru}(\text{dppz})_2\text{phen}](\text{PF}_6)_2$ (compound **3**) and $[\text{Ru}(\text{dppn})_2\text{phen}](\text{PF}_6)_2$ (compound **4**) were more problematic, mainly due to solubility issues of the precursors. We first tried to synthesize the compounds starting from the $\text{Ru}(\text{LL})\text{Cl}_2$ precursor, followed by coordination with phen, as previously reported in literature,²³ but tedious purification steps were necessary to obtain the desired compounds in low yields. One of the main problems related to the synthesis was the insolubility of the precursor $[\text{Ru}(\text{LL})\text{Cl}_2]$, that did not allow for characterisation or purification. Therefore, we envisioned a different synthetic route starting from the coordination of two phendione ligands to the precursor $[\text{Ru}(\text{DMSO})_4\text{Cl}_2]$ in anhydrous DMF, to obtain the corresponding di-substituted Ru(II) di-chloro compound $[\text{Ru}(\text{phendione})_2\text{Cl}_2]$, followed by the coordination of the phen ligand in EtOH/H₂O (1/1, v/v). As expected, the intermediate could be isolated by precipitation as PF_6^- salt and directly used in the following step without the need of any chromatographic purification. Finally, the intermediate $[\text{Ru}(\text{phendione})_2\text{phen}](\text{PF}_6)_2$ was reacted with an excess of o-phenylenediamine in CH₃CN/EtOH (1/3, v/v) to obtain the final compound **3** or **4** after precipitation with NH_4PF_6 . Remarkably, there was no need to purify the product by column chromatography, but just by filtration and washing with water, obtaining yields of 82% and 55% for compound **3** and **4**, respectively (**Scheme 1**). This modified synthetic pathway allowed to improve the yields described in the literature, and therefore made it possible to study this attractive class of compounds.



Scheme 1: synthetic scheme for the four compounds synthesized in this work.

X-ray Crystallography

Single crystals of **1** and **3** were obtained by dissolving the compounds in CH_3CN , followed by slow addition of diethyl ether to allow solvent diffusion. The structures of the cations of the compounds are shown in **Figure 2**. As expected, both complexes are constructed around the RuN_6 core, where the metal centre is characterised by an octahedral geometry. No substantial differences in terms of bond lengths or angles were observed compared to already described $\text{Ru}(\text{II})$ trispolypyridyl complexes.²⁷ Interestingly, both compounds show π - π stacking (**Figure SI18-19**). On one hand, the phen ligand of **1** seems to be intercalated between the two DIP ligands of proximal molecules. On the other hand, the intercalation of the dppz ligands of **3** is much more pronounced, which was not surprising since the aromatic structure of the dppz ligand is longer than the DIP, allowing a better π - π interaction (**Figure SI19**). The steric hindrance caused by the phenyl substituents of the DIP ligand probably contribute to decrease the π - π stacking among the DIP ligands too.

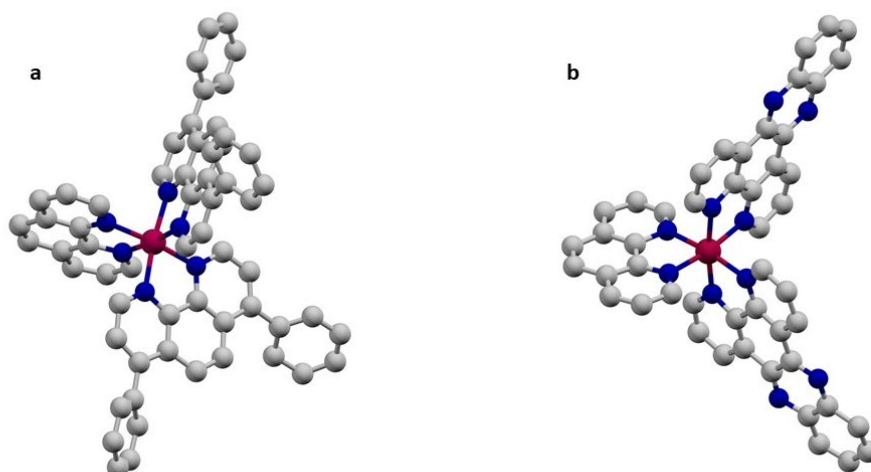


Figure 2: Solid state structures of cations of **1** (a) and **2** (b) obtained by X-Ray diffraction of single crystals. Ru atoms are in magenta, N atoms in blue and C atoms in grey. H atoms, solvent atoms, counterions and disordered atoms in the structure are omitted for clarity.

Absorption and Emission properties of the Ru(II)-complexes

The UV-Vis absorption spectra in CH₃CN were then recorded and are showed in **Figure 3**. The maximum absorption wavelength of a PS is a very important parameter since it determines the wavelength to be used for its photoactivation. In this sense, the use of long-wavelength light (500-900) is generally preferred since it has deeper tissue penetration, which is required for a PDT treatment to be effective, especially in *in vivo* and clinical settings.²⁸ Compounds **1** and **2** displayed two bands in the UV range (273 and 276 nm), corresponding to the spin-allowed π - π^* transitions. The shoulder around 320 nm is ascribed to the ¹MLCT and ¹LLCT.²⁹ The broad band between 350 and 510 nm corresponds to the metal to ligand charge transfer (¹MLCT transition). Compound **3** presented an intense intraligand π - π^* transition centred at 280 nm, while the one of compound **4** is shifted at 290-340 nm. Moreover, for **4** this transition gives a double humped absorption at 389 and 410 nm. A broad ¹MLCT band is centred at 435 nm.²⁴

1-3 are also characterised by an emission band after excitation at 450 nm in CH₃CN, while **4** does not emit in these conditions, according with what reported by Giorgi *et al.* for similar compounds (**Table 1, Figure S120**).²⁴

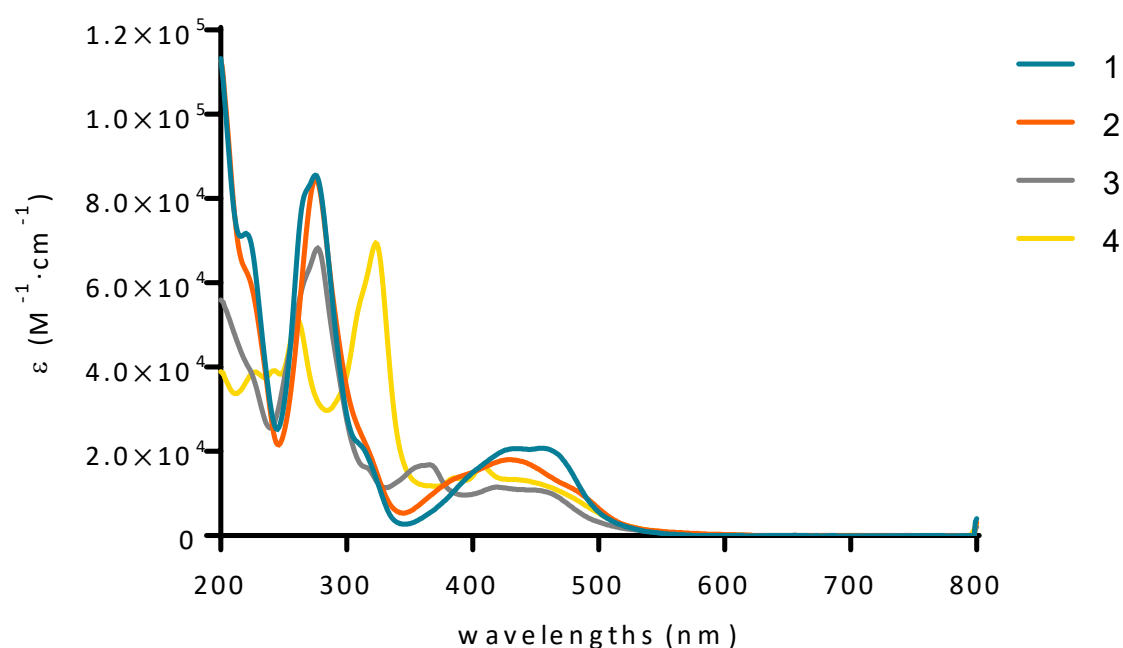


Figure 3: UV-Vis spectra of compounds **1-4** in CH₃CN. The solutions have been prepared in CH₃CN and used at the following concentrations: 10.4 μM (**1**), 14.8 μM (**2**), 15.5 μM (**3**), 12.5 μM (**4**).

Distribution coefficient (*LogP* values)

The octanol-water partition coefficient (*LogP*) is an important parameter for drugs, as it highly affects the cellular uptake by passive diffusion.³⁰ We employed the “shake-flask” method³¹ to measure the *LogP* values of **1-4** (Table 1). As expected, the compounds showed *LogP* values between 1 and 1.5, indicating that the compounds are hydrophobic. Moreover, we can observe that all the compounds have similar *LogP* values.

Compound	Absorption maxima λ (nm) ^a	Emission maxima λ (nm) ^a	$\log P^b$
1	222, 273, 442	608	1.5 ± 0.3
2	222, 276, 435	682	1.6 ± 0.3
3	222, 275, 363, 435	612	1.0 ± 0.2
4	222, 242, 261, 325, 435	n.d.	1.3 ± 0.1

Table 1: Absorption maxima, emission maxima and *LogP* values of the ruthenium complexes. ^aUV-Vis spectra and emission spectra recorded in CH₃CN. ^bExperimentally determined using the shake-flask method.

(Photo)-stability Studies

In some cases, PSs can undergo degradation after light irradiation causing the release of toxic moieties.³² To evaluate the photo-stability of the complexes **1-4**, the evolution with time of their absorption properties was monitored through UV-Visible spectroscopy during continuous irradiation at 540 nm (9 J/cm²). Very interestingly, the absorption spectra of all the synthesized Ru(II) derivatives in CH₃CN remained unchanged after 40 min of light irradiation, demonstrating that no photodegradation occurred (**Figure SI22**). The decrease in absorption intensity observed in the UV-Vis spectra of compound **4** was attributed to the presence of aggregation phenomena, which have previously been reported in the literature for similar compounds.^{33,34} CH₃CN was used since the poor solubility of the compounds in water did not allow to obtain the suitable concentration for the UV-Vis analysis. Next, the stability of the complexes in DMSO was investigated. For this purpose, ¹H-NMR spectra of compounds **1-4** were recorded over a period of 48 h (**Figure SI23-26**). Overall, the compounds showed a remarkable stability since no changes in the spectra were observed.

Singlet oxygen quantum yield

The PS, after excitation with light, is excited to an unstable singlet state *S*₁, which can release the excess of energy by luminescence, or by non-radiative relaxation. The most important electronic transition involved in PDT is the intersystem crossing (ISC), which leads to an excited triplet state *T*₁, that presents a longer lifetime than the excited singlet state *S*₁. The excited *T*₁ state can decay by radiative relaxation, giving phosphorescence, or interacting with other species present in the biological environment. This, in turn, generates ROS, responsible for the activation of different cell death pathways. Another mechanism involves molecular oxygen (³O₂) that is excited by energy transfer from the excited *T*₁, leading to the formation of ¹O₂. ¹O₂ presents a very short life-time (<0.04-3 μs) and a very high reactivity, allowing a spatio-temporal control of its area of action (0.01-0.155 μm).^{12,35} In this context, it is clear that the PS' efficacy of triggering the formation of ¹O₂ species after excitation by light is very important for the efficiency of the PS in PDT. The measurement of ¹O₂ quantum yield is of main importance to evaluate if a PS can exploit the light

energy to convert $^3\text{O}_2$ to the reactive singlet oxygen species $\text{O}_2 (^1\Delta\text{g})$.^{2,3,12} Therefore, we evaluate the photophysical properties of the compounds and their $^1\text{O}_2$ quantum yield.

1-3 present similar emission spectra after excitation at 450 nm, with an emission band around 600 nm for **1** and **3**, and 682 nm for **2** (**Figure S120**). On the contrary, compound **4** does not emit at all, with a luminescence quantum yield of 0 (**Table 2**).

Compound	Luminescence quantum yield	Luminescence lifetime (ns)	$^1\text{O}_2$ quantum yield
1	0.06	179	0.60
2	0.08	371	0.36
3	0.16	188	0.37
4	0.00	n.d.	0.73
[Ru(bpy)₃]Cl₂	0.08	159	0.57

Table 2: Photophysical properties of the compounds **1-4** in CH_3CN .

In this context, the $^1\text{O}_2$ quantum yield of the four Ru complexes was measured in aerated CH_3CN using $[\text{Ru}(\text{bpy})_3]\text{Cl}_2$ as standard. To our delight, compounds **1-3** showed moderate to high $^1\text{O}_2$ quantum yields, with values ranging from 0.36-0.73. Remarkably, compound **4** showed a $^1\text{O}_2$ quantum yield of 0.73 (**Figure S122**). The lack of luminescence of compound **4** together with a high $^1\text{O}_2$ quantum yield suggest that most of the energy of the T_1 excited state of **4*** is used to produce $^1\text{O}_2$.

DNA thermal denaturation and Photocleavage Studies

The polypyridyl Ru(II) compounds have been intensively studied for their application as DNA intercalators.³⁶⁻³⁸ In this work, we focused our interest in understanding if the synthesized compounds are able to bind the duplex DNA, and how this interaction can influence the stability of the DNA duplex. As previously demonstrated by Cardin and co-workers, the intercalation of a polypyridyl metal complex on the duplex DNA depends not only on the metal derivative, but also on the different sequences and the different steps of the DNA sequence. In particular, they observed by crystal structure analysis that the dppz ligand of the compound $\Lambda\text{-}[\text{Ru}(\text{phen})_2(\text{dppz})]\text{Cl}_2$ intercalates symmetrically and perpendicularly from the minor groove of the $d(\text{CCGGTACCGG})_2$

duplex at the central TA/TA step.³⁹ [Ru(phen)₂(dppz)]Cl₂ was described as a stabilising agent for the duplex structures of RNA and DNA.⁴⁰ In this work, we studied the effect on the thermal stability of dsDNA after ruthenium interaction, using the CD thermal denaturation method to determine the difference of melting point after addition of 1 or 2 equivalents of compound **3** to different DNA sequences. Unfortunately, it was not possible to evaluate the DNA interaction of the other compounds since precipitation occurred even with 1:1 ratio of DNA:compound. This appeared only when the compound was added to the DNA solution and not in the absence of DNA. Since **3** was the only compound which could be solubilised to the concentrations necessary for the experiment, it was taken as model even if no colocalization in nuclei or mitochondria was observed by the studies reported below. Sequences were chosen based on their differences in terms of base steps, to evaluate how the interaction is influenced by changing the sequence. We selected two sequences of dsDNA d(CCGGTACCGG)₂ (TA) and d(CCGGCGCCGG)₂ (CG), and for each sequence we used a DNA:Ru ratio of 1:1 or 1:2. After increasing the temperature from 10 to 80°C with 5°C increments, we observed shifts of the melting transitions to higher temperatures (**Figure 4**). In particular, both sequences were stabilised by addition of the compound. Interestingly, for the TA sequence we can observe that the DNA is more stabilised with 1:1 ratio, while adding complex equivalents lead to a decreased stabilising effect (**Figure 4**). Overall, the results indicate that there is a preference in terms of step for the interaction, and that the presence of two bulky ligands instead of only one does not probably change the DNA binding. Overall, these results confirm the stabilising effect of the Ru(II) derivatives bearing dppz ligands. This study is a preliminary step in the investigation of the interaction of **3** with different DNA sequences, and a more detailed investigation is needed to unravel their interaction and determine any sequence selectivity and/or specificity of binding and stabilisation.

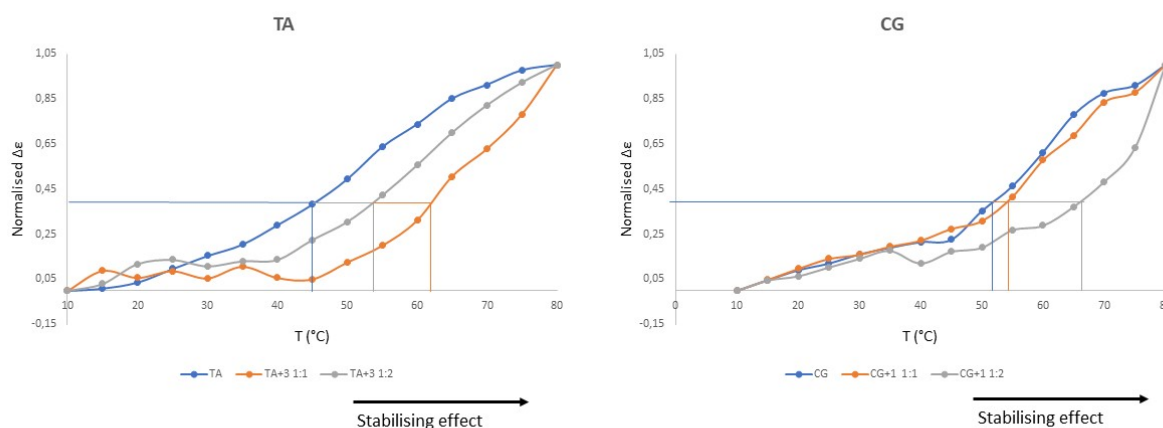


Figure 4: dsDNA melting curve with DNA:compound ratio of 1:0 (blue line), 1:1 (orange line), 1:2 (grey line). Conc. of dsDNA was 40 μM , conc. of **3** was 40 or 80 μM . Melting curves were recorded from 10 to 80°C, holding time 1 min, 1°C/min and recorded CD each 5°C change in temperature. Each graph is representative of at least two independent experiments.

After obtaining the DNA stabilising results, we also tried to investigate the ability of the compounds to cleave the DNA after light activation. Unfortunately, as observed for the stability studies by melting curves, the compounds were precipitating once the DNA in the duplex, single strand, G-quadruplex or plasmid form were added to the solution. Therefore, it was not possible to obtain any reliable result (data not shown). We hypothesised that the strong interaction of the compound with DNA might cause an unbalance of DNA charges that leads to the precipitation of the DNA in the presence of the Ru(II) complexes.

(Photo-)Toxicity Studies

To evaluate the biological activity of the four compounds, we performed a 2D *in vitro* viability assay against two cancerous cell lines CT26 (mice colon adenocarcinoma), HT29 (human colorectal adenocarcinoma), and one non-cancerous cell line RPE-1 (eye pigmented retinal epithelium). Their cytotoxicity in the dark and upon light irradiation at different wavelengths (i.e., 540, 595 and 620 nm) was investigated using a fluorometric cell viability assay. In all the experiments, Protoporphyrin IX (PpIX) was used as positive control. Since it is known that UV light can cause cell death,⁴¹ it is important to mention that the light dose was carefully optimised in order to have a cell survival of

non-treated cells of at least 95 % after light irradiation. After adjustment of the irradiation time, the phototoxicity of the compounds was evaluated in the different cell lines. Very promisingly, all the tested compounds were non-toxic in dark conditions up to 100 μM and were very toxic after light irradiation at 540 nm, with IC_{50} values in the range 0.06-7 μM . Since one of the main issues of PDT is low light tissue penetration, there is much interest in finding PSs able to cause a phototoxic effect after activation with longer wavelengths, allowing for a deeper tissue penetration.²⁸ For this reason, we tested the compounds' phototoxicity also after excitation at 595 nm and 620 nm (3.4 and 6.7 J/cm^2 , respectively). Viability results showed that the compounds were generally less phototoxic when irradiated with longer wavelengths than after irradiation at 540 nm, with no toxicity at all for compound **3**. This could be explained by the better luminescence quantum yield of compound **3**, with a lifetime of 188 ns, and a low $^1\text{O}_2$ quantum yield as compared to compound **4** and $[\text{Ru}(\text{bpy})_3]\text{Cl}_2$, which was used as the standard. Overall, these results could indicate that **3** dissipates energy by luminescence, losing its PDT activity. However, encouraging results have been obtained with compound **4**, displaying very low IC_{50} values at all the studied wavelengths. Importantly, this compound showed similar or even better IC_{50} values compared to the control (PpIX). Concerning **1** and **2**, the IC_{50} values showed a better activity as compared to **3**. Anyway, the phototoxic activity decreased drastically after irradiation at 620 nm. The different activity between **1** and **2** compared to **3** could be explained by the luminescence quantum yield and the $^1\text{O}_2$ quantum yield. As we suggested, the poor activity of compound **2** and **3**, could be the consequence of the low $^1\text{O}_2$ quantum yield. However, the luminescence quantum yield of **2** is much lower than **3**, suggesting that the excited triplet state directly dissipate energy by producing ROS. **1** is characterised by a low emission, but a very good $^1\text{O}_2$ production, which once again can explain the better activity of **1** and **2** as compared to **3**. Interestingly, no activity of compound **3** was observed after irradiation at 540 nm on HT29 cells, indicating that compound **3** is more toxic against CT26 cells rather than HT29. However, there was no selectivity towards cancer cells rather than healthy cells.

Overall, all the Ru(II) derivatives displayed higher toxicity after excitation at 540 nm, while lower phototoxic effect was obtained with 595 nm and 620 nm. The compounds do not have any selectivity against cancer cells if compared to non-cancerous cells (**Table 3**). Remarkably, **4** displayed a very promising IC_{50} at all irradiation wavelengths, with no toxicity in dark and, therefore, high PI (Phototoxicity Index).

540 nm	595 nm	620 nm
--------	--------	--------

<i>CT26</i>									
Compound	IC₅₀ dark	IC₅₀ light	PI	IC₅₀ dark	IC₅₀ light	PI	IC₅₀ dark	IC₅₀ light	PI
1	>100	0.09 ± 0.05	1111	>100	8 ± 1	13	>100	10 ± 1	10
2	>100	2.8 ± 0.1	36	>100	23 ± 3	4	>100	37 ± 16	3
3	>100	7 ± 6	14	>100	>100	1	>100	>100	/
4	>100	0.06 ± 0.02	1666	>100	1.9 ± 0,7	53	>100	0.75 ± 0.03	133
PpIX	>100	0.12 ± 0.04	833	>100	8.8 ± 0.3	11	>100	0.51 ± 0.06	196
<i>HT29</i>									
1	>100	1.6 ± 0.1	63	>100	3.2 ± 0.7	31	>100	32,5 ± 0.7	3
2	>100	1.5 ± 0.5	67	>100	20 ± 15	5	>100	31 ± 1	3
3	>100	>100	/	>100	>100	/	>100	>100	/
4	>100	0.18 ± 0.08	556	>100	0.4 ± 0.2	250	>100	2.5 ±0.4	40
PpIX	>100	1.1 ± 0.6	91	>100	0.7 ± 0.5	143	>100	2.9 ± 0.6	34
<i>RPE-1</i>									
1	>100	0.9 ± 0.2	111	>100	7.8 ± 0.4	13	>100	17 ± 3	6
2	>100	1.4 ± 0.3	71	>100	19 ± 4	5	>100	13 ± 2	8
3	>100	9 ± 4	11	>100	>100	/	>100	>100	/
4	>100	0.18 ± 0.02	556	>100	1.3 ± 0.4	77	>100	0.3 ± 0.2	333
PpIX	>100	0.5 ± 0.2	200	>100	0.9 ± 0.1	111	>100	0.26 ± 0.08	385

Table 3: (Photo)-toxicity IC₅₀ (μM) values towards CT26, HT29 and RPE-1 at 540 nm (9 J/cm²), 595 nm (3.4 J/cm²), and 620 nm (6.7 J/cm²). The reported values were obtained as mean of three independent experiments.

Cellular internalisation by confocal microscopy and ICP-MS

A drug's activity and efficacy rely on the drug cellular uptake. Moreover, the accumulation in different organelles could lead to a variation in drug activity.⁴² Therefore, we decided to investigate the internalization of the tested compounds using confocal microscopy, particularly focusing on nuclear and mitochondrial accumulation. Compounds **1-3** were easily visualized following excitation at 448 nm, whereas the dppn derivative **4** was not included in this study, since it did not show any luminescence after excitation. Nuclear and mitochondrial accumulation was assessed using co-labelling with the DNA nuclear stain Hoechst 33342 and the live mitochondria stain MitoTracker™ DeepRed. As shown in Figure 5, none of the compounds showed detectable accumulation in the nucleus, as confirmed by the negative values of Pearson coefficients between Hoechst signal and compounds **1**, **2** and **3** (-0.27, -0.35, -0.17 respectively).

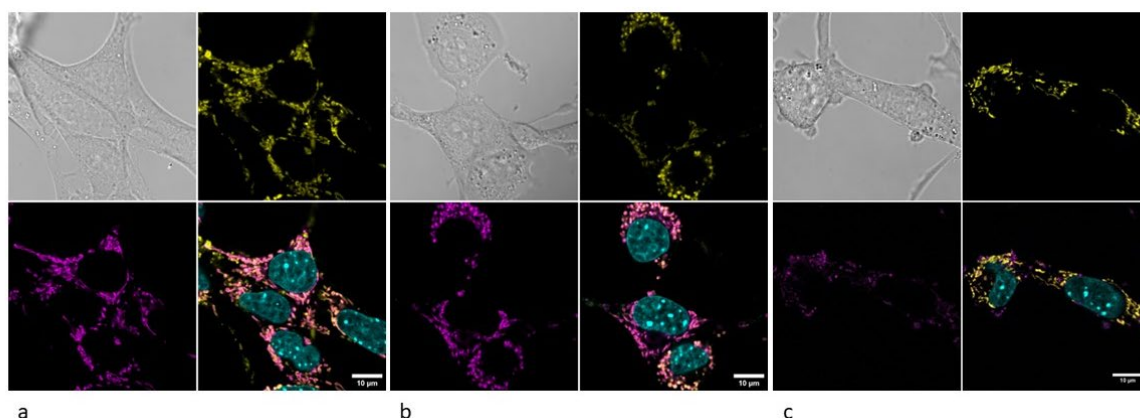


Figure 5: Subcellular localization of compounds **1** (a), **2** (b), and **3** (c) by confocal microscopy. CT26 cells were imaged live following incubation with the compounds (10 μ M) for 4 h, then with Hoechst 33342 and MitoTracker™ Deep Red for 10 min. In each picture, the top left panel is the bright field image, the top right panel is the MitoTracker signal (yellow), the bottom left panel is the compound signal (magenta) and the bottom right panel is the merge of fluorescent channels.

Mitochondria are pivotal organelles in cell apoptosis. In particular, oxidative stress can trigger the mitochondria-dependent cell death signalling pathway.⁴³ Some Ru(II) polypyridyl compounds can selectively target mitochondria, as previously reported by Chao and co-workers.⁴⁴ However, although these compounds showed high phototoxicity after light irradiation, they also had

important toxicity in the dark, likely because they affect redox homeostasis within mitochondria and thus cellular energy production.⁶ Interestingly, **1** and **2** were found to significantly and similarly accumulate in mitochondria (**Figures 5a, 5b**), with Pearson coefficient values of 0.56 and 0.65 respectively between compounds and MitoTracker™ fluorescence signals. Of note, the compounds presented no toxicity in the dark, indicating that they affect mitochondria only after light irradiation. Previous studies showed accumulation in mitochondria of similar Ru(II) compounds with DIP ligands,⁶ confirming what we observed in the present study for **1** and **2**. By contrast, the luminescence of compound **3** did not show any overlap with MitoTracker™ (Pearson coefficient value of -0.15), suggesting that its phototoxicity upon light excitation does not involve its accumulation in mitochondria (**Figure 5c**). Moreover, the intracellular fluorescence signal from compound **3** was very low, likely because this compound is weakly internalized after 4 h treatment, as revealed by ICP-MS analysis (**Figure SI39**).

To have a better understanding of the subcellular localization of the non-luminescent compound **4**, we used ICP-MS on purified mitochondria. Compound **1** was also included in this study as a positive control. Interestingly, almost 40% of the internalized compound **1** localized in mitochondria (**Figure 6b**), in line with what we observed by confocal microscopy. By contrast, less than 5% of the compound **4** accumulated in mitochondria, despite a higher cellular uptake compared to **1** (**Figure 6 and SI40**). It is interesting to notice that compounds **1** and **2**, which bear the DIP ligands, accumulate in mitochondria, while **3** and **4**, which have dppz or dppn ligands, do not significantly localize in these organelles.

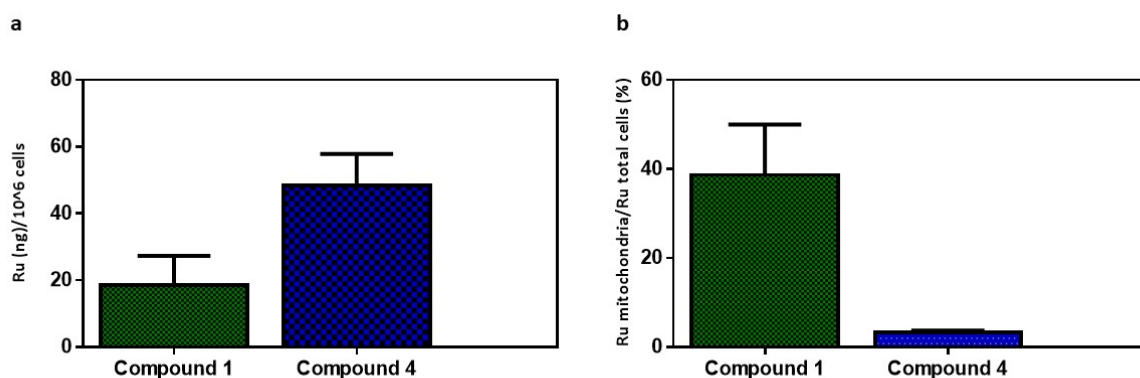


Figure 6: Whole cell and mitochondrial accumulation of compounds **1** and **4** following overnight incubation of CT26 cells with compounds **1** or **4** (1 μ M) assessed by Ru quantification using high-

resolution ICP-MS. (a) Whole cell accumulation. (b) Fraction of the whole cellular content accumulated in mitochondria.

Metabolic Studies of mitochondria respiration

According to our results on mitochondria internalisation of **1** and **2**, we decided to compare the impact of our best compounds (**1** and **4**), on the cellular respiration, using a Seahorse XF analyser. Mitochondria are cellular organelles responsible for the ATP production by oxidative phosphorylation. They also have important roles in several metabolic pathways, in apoptosis and programmed cell death, and in ROS homeostasis.^{45,46} In cancer cells, mitochondrial function is essential and plays a central role for the cell viability.⁴⁷ The Seahorse assay was used to investigate the effect of the tested compounds on the mitochondrial respiration, and to elucidate if the accumulation of our compounds in the mitochondria could influence the cellular respiration. Cells were treated for 4 h with the compounds using their IC₅₀ and IC₂₅ concentration, and then irradiated at 540 nm for 40 min. After degassing the culture medium for 1 h in a non-CO₂ incubator, the cells were treated with sequential injections of specific inhibitors of the electron transport chain. First, oligomycin was added to inhibit the ATP synthase, FCCP (carbonyl cyanide 4-(trifluoromethoxy)phenylhydrazone) was then added as an uncoupling agent that induces maximal oxygen consumption rate (OCR), and a combination of Rotenone/Antimycin A was injected to block the electron transport chain, to stop the mitochondrial O₂ consumption. The Mito Stress Test was performed following the Agilent protocol.⁴⁸ Our Seahorse results showed that despite the fact that compound **1** showed mitochondria internalisation by confocal microscopy studies, almost no effect on the cellular respiration was observed at IC₂₅ and IC₅₀ concentrations. On the contrary, we observed a severe impairment of mitochondrial respiration in samples treated with **4** together with irradiation at 540 nm for 40 min, while no effect was observed in cells kept in dark condition. Compound **4** clearly affect not only the ATP-linked respiration but also the spare capacity (**Figure 7a**). In **Figure 7b**, we can clearly see that the respiration capacity is diminished by the administration of compound **4**. Overall, **4** is the most effective, inducing a decrease in respiration higher than that of the positive control PpIX. It is worth to mention that PpIX impaired mitochondrial respiration either in the dark or light conditions, while **1** and **4** showed values similar to the negative control in dark. Our results suggested that the dysregulation of the mitochondrial respiration is one of the cell death mechanisms driven by compound **4**. This could be due to depolarisation of the mitochondrial

membrane. In fact, previous studies have shown that Ru(II) polypyridyl compounds can trigger mitochondrial depolarization independently from their cellular sub-localisation.^{49,50}

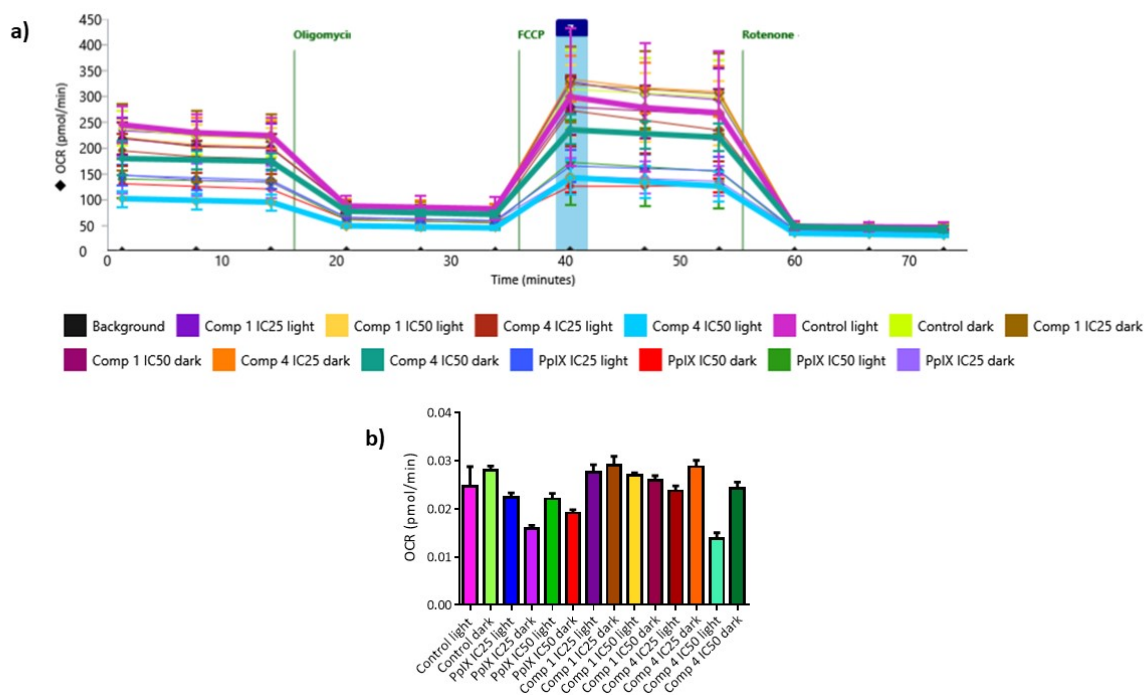


Figure 7: (a) MitoStress test OCR profile in CT26 cells after 4 h of treatment and 40 min of irradiation. Oligomycin (inhibitor of ATP synthase), FCCP (uncoupling agent), antimycin-A (complex III inhibitor), and rotenone (complex I inhibitor) were sequentially added. The OCR profile of compound **4** (IC₅₀ light and dark) and control light are highlighted in the graph. The blue bar indicates the time spot at which we registered the bar graph below. (b) Bar Graph of the OCR profile of each compound after injection of FCCP (t = 40 min).

Conclusions

In summary, in this work, we report on the synthesis, characterization and biological evaluation of four Ru(II) polypyridyl compounds. An alternative synthetic method to obtain the Ru(II) derivatives bearing two dppz or dppn ligands in good yields is described. The four compounds displayed an excellent stability in DMSO over 48 h, and in CH₃CN after light irradiation at 540 nm for 40 min. Very promising phototoxicity properties against different cancer cell lines were observed. In particular, compound **4** stands out for its photo-activity in the micro- or even nanomolar range at all the tested wavelengths, making this compound very interesting for PDT applications. The interaction with different sequences of DNA has been studied taking as model compound **3**. Interestingly, a DNA

stabilising effect was observed, which is consistent with the one proposed for the largely studied compound $[\text{Ru}(\text{phen})_2(\text{dppz})]\text{Cl}_2$. In addition, the internalisation of these Ru(II) derivatives in organelles containing DNA, i.e. nuclei and mitochondria, was investigated. None of the compounds entered the nuclei, but compounds **1** and **2** targeted the mitochondria. Moreover, to study the mechanism of action of the best performing compounds **1** and **4** we evaluated their ability in affecting the cellular respiration. Very interestingly, compound **4** affected the mitochondrial respiration only after light exposure, while no consistent effect was observed in dark condition. Overall, this work shed light on the promising phototoxic activity of the tested compounds and their interaction with important biological targets such as mitochondria and DNA.

Materials and methods

All chemicals were purchased from commercial sources and used without further purification. If necessary, solvents were dried over molecular sieves. The Ru(II) precursors $\text{Ru}(\text{DMSO})_4\text{Cl}_2$ and $\text{Ru}(\text{DIP})_2\text{Cl}_2$ and $\text{Ru}(\text{phendione})_2\text{Cl}_2$ were synthesized following previously reported procedures.^{51,52} The cell culture media and reagents were purchased from Fisher Scientific. Thin layer chromatography (TLC) was performed using silica gel 60 F-254 (Merck) plates with detection of spots by exposure to UV light. Eluent mixtures are expressed as volume to volume (v/v) ratios. ^1H - and ^{13}C -NMR spectra were measured on Bruker Avance III HD 400 MHz or Bruker Avance Neo 500 MHz spectrometers. The deuterated solvent signal was used as an internal standard. The chemical shifts δ are reported in ppm (parts per million) relative to tetramethylsilane (TMS) or signals from the residual protons of deuterated solvents. The following abbreviations were used to designate multiplicities: s = singlet, d = doublet, t = triplet, m = multiplet, dd = double-doublet. ESI experiments were carried out using a 6470 Triple Quad (Agilent Technologies). HPLC analysis was performed using two Agilent G1361 1260 Prep Pump, an Agilent G7115A 1260 DAD WR detector equipped with an Agilent Pursuit XRs 5C18 (100 Å, C_{18} 5 μm 250 \times 4.6 mm) column. The flow rate was 1 mL/min with the following gradient: 0–3 min: isocratic 95% A (5% B); 3–17 min: linear gradient from 95% A (5% B) to 0% A (100% B); 17–23 min: isocratic 0% A (100% B). Chromatograms were detected at 250 nm. The solvents (HPLC grade) were Millipore water (solvent A) and acetonitrile (solvent B). Only for compound **1** we used 0.1% v/v of trifluoroacetic acid in A and B. The samples were dissolved in CH_3CN and filtered through a 0.2 mm membrane filter before the injection. The absorption spectra were measured with an Agilent Cary UV-visible Multicell Peltier spectrophotometer. The luminescence spectrum was measured with a Fluorolog FL3-222 spectrofluorimeter (Horiba Jobin

Yvon, Palaiseau, France) equipped with a 450 W xenon arc lamp, with a thermostatically controlled cell holder compartment (25°C), a UV-visible photomultiplier tube R928 (HAMAMATSU Japan) and an infrared detector InGaAs cooled by liquid nitrogen (DSS-IGA 020L Electro-Optical System Inc, Phoenixville, PA, USA). The excitation beam is separated by a SPEX dual network monochromator (1200 lines / mm blazed at 330 nm). The luminescence was measured by the UV-Visible detector via the SPEX dual network emission monochromator (1200 lines / mm blazed at 500 nm). $^1\text{O}_2$ luminescence was measured with an infrared detector InGaAs (800 - 1550 nm) via the dual network emission monochromator SPEX (600 lines / mm blazed at 1 μm). The cell culture medium and DNA plasmid were purchased from Thermo Fischer. DNA sequences for thermal studies were provided by Eurogentec.

X-ray crystal structures

Single crystals were grown in $\text{CH}_3\text{CN}/\text{Et}_2\text{O}$ at 18°C. A suitable crystal was selected and mounted in a loop on a Synergy diffractometer. The crystals were kept at 100 K during data collection. Using Olex2,⁵³ the structures were solved with the SHELXT⁵⁴ structure solution program using intrinsic phasing and refined with the SHELXL⁵⁴ refinement package using least squares minimization. Full details are included as supplementary information.

Stability Studies in DMSO

The stability in DMSO-d_6 at 37°C was assessed by $^1\text{H-NMR}$ over 48 h. Spectra were recorded at time zero, 1 h, 6 h, 12 h, 24 h and 48 h.

Measurement of octanol-water partition coefficient (log *P*)

The log *P* values were determined using the shake-flask method. 1 mL of octanol was pre-saturated with 1 mL of PBS by overnight incubation with shaking of a biphasic mixture of the two at room temperature. 5 μL of a 10 mM DMSO stock solution of each compound was added into the biphasic solution of PBS/octanol to give a final concentration of 50 μM . The mixture was shaken for 24 h using an automated shaker and allowed to stand for 2 h. Aliquots from the octanol phase and the aqueous phase were extracted and analysed using the UV-Vis detector to determine their relative concentrations in each phase. The measurements were repeated three times for each complex.

Photostability

The photostability of the tested compounds was evaluated by irradiation at 540 nm in 96 well plates with an Atlas Photonics LUMOS BIO irradiator during time intervals from 0-40 min. UV-Vis spectra were recorded using the BioTek Cytation 5. The solutions were prepared in air saturated CH₃CN at 100 μM, and read after different times of irradiation (i.e., 0 min, 10 min, 20 min, 30 min, 40 min).

Singlet oxygen and luminescence quantum yield

All spectra were measured using 4-sided quartz cells. The absorption values of the references and samples at the excitation wavelength were adjusted to 0.2. All emission spectra were normalized to the same absorbance for the purpose of comparison. [Ru(bpy)₃]Cl₂ in acetonitrile was chosen as standard for both luminescence and ¹O₂ quantum yield determination. Luminescence quantum yield of [Ru(bpy)₃]Cl₂ in CH₃CN is evaluated at 0.077.⁵⁵ ¹O₂ quantum yield of [Ru(bpy)₃]Cl₂ in aerated CH₃CN is evaluated at 0.57.⁵⁶ Time-resolved experiments were performed using for excitation: a pulsed laser diode emitting at 407 nm (LDH-P-C-400M, FWHM < 70 ps, 1 MHz) coupled with a driver PDL 800-D (both PicoQuant GmbH, BERLIN, Germany) and for detection: an avalanche photodiode SPCM-AQR-15 (EG & G, VAUDREUIL, Canada) coupled with a 650 nm long-wave pass filter as detection system. The acquisition was performed by a PicoHarp 300 module with a 4 channels router PHR-800 (both PicoQuant GmbH, BERLIN, Germany). The luminescence decays were recorded using the single photon counting method. Data were collected up to 500 counts accumulated in the maximum channel and analysed using Time Correlated Single Photon Counting (TCSPC) software Fluofit (PicoQuant GmbH, BERLIN, Germany) based on iterative reconvolution using a Levensberg- Marquandt algorithm, enabling the obtention of multi-exponential profiles (mainly one or two exponentials in our cases).

Solution preparation for annealing

Initial stock solutions of the ruthenium complexes were made in EtOH, and oligonucleotides were made in water. The concentration of the solutions was checked using the extinction coefficient of 20 000 M⁻¹ cm⁻¹ at 450 nm for the Ru compound, and the Eurogentec-provided extinction coefficients at 260 nm, calculated using the nearest-neighbour model, were used for DNA. The stocks were then diluted with buffer and combined to form solutions with either 1:1 or 1:2 ratio of

DNA strands to ruthenium complex. Annealing of the oligonucleotides, both with and without ruthenium complex present, was carried out by incubating the buffered solution at 90°C for 5 min, and then allowing it to cool to room temperature.

CD Thermal Denaturation

CD melting experiments were carried out using Chirascan V100 with a temperature controlled four-cell changer. Samples were prepared at a concentration of 40 μM of DNA and either 1 or 2 molar equivalents of the ruthenium complex. The buffer consisted of 50 mM sodium cacodylate at a pH 7. Absorption was recorded at 260 nm at 5°C intervals between 10–80°C, with a temperature change rate of 1 °C/min in a 0.1 cm pathlength quartz cuvette. Melting curves were generated from this data.

Cell culture

CT26 cells were cultured in DMEM media (Gibco, Life Technologies, USA), HT29 cells were cultured in McCoy 5 and RPE-1 cells were cultured in DMEM/F-12 (Gibco) supplemented with 10 % of fetal bovin serum. All cell lines were complemented with 100 U/mL penicillin streptomycin mixture (Gibco) and maintained in humidified atmosphere at 37 °C and 5 % of CO₂.

2D (Photo)-toxicity Assay

(Photo)-toxicity of compounds **1-4** and PpIX in dark and light conditions was carried out by a fluorometric cell viability assay using Resazurin (ACROS Organics). Cells were seeded in triplicate in 96-well plates at a density of 4×10^3 cells/well (for CT26) or 6×10^3 cells/well (for HT29 and RPE-1) in 100 μL of culture media. After 24 h of incubation at 37°C with 5% CO₂, cells were treated with increasing concentrations of the ruthenium complexes. Dilutions were prepared from a 10 mM stock solution in DMSO, which was further diluted to different concentrations (0.01-100 μM) in cell media. After 4 h of incubation with the tested compounds, the medium was replaced with fresh medium, and the cells were irradiated for a variable time depending on the wavelength (40 min at 540 nm with irradiance of 9 J/cm², and 1 h at 595 and 620 nm with irradiance of 3.4 J/cm² and 6.7 J/cm², respectively). Cells were incubated up to 48 h. Then, 100 μL of complete medium containing resazurin (0.2 mg/mL final concentration) was added. After incubating for 4 h at 37 °C, the

fluorescence signal of resorufin product was read (ex: 540 nm em: 590 nm) in a BioTek Cytation 5 fluorimeter. IC₅₀ values were then calculated using GraphPad Prism software 9. XY analysis with three replicate values in side-by-side sub columns was chosen. Inserted raw data obtained from BioTek Cytation 5 fluorimeter was treated as follows: X values were transformed to the logarithm and data were normalized to the lowest Y value. Data were then analysed with “Nonlinear regression” (curve fit) and then “log(inhibitor) vs. normalized response”.

Subcellular localization by confocal microscopy

CT26 cells (3×10^4 cells/well) were seeded in 35 mm culture dishes with 20 mm diameter glass coverslip bottom and incubated for 48 h. Cell medium was then replaced by fresh medium containing 10 μ M of **1-3**. After incubation for 4 h in the dark at 37°C with 5% CO₂, cells were washed with PBS to remove the compound not internalized in the cells. Cells were stained with Hoechst 33342 (1 μ g/mL) and MitoTracker™ Deep Red (MTDR, 100 nM) at 37°C for 10 min. Live cells were imaged in a confocal laser scanning microscope SP8 (Leica Microsystemes, Nanterre, France) equipped with a x63/1.40 plan apochromat objective. The excitation/emission wavelengths were 405/420-450 nm (Hoechst), 448/600-650 nm (**1-3**) and 638/660-700 nm (MTDR). Laser intensities were kept as low as possible to avoid any phototoxicity. To quantify the amount of colocalization between each compound and Hoechst or MTDR, Pearson coefficients were calculated using the coloc2 plugin in ImageJ software.

Sample preparation for cellular fractionation

CT26 cells were seeded at a density of 2×10^6 in 10 cm plates and incubated for 24 h at 37°C with 5% of CO₂. Cells were treated with 1 μ M concentration of compound **1** and **4**. After overnight incubation, cells were washed 2x with 5 mL of cold PBS, collected, counted, and the Sigma Mitochondria Isolation Kit protocol (MITOISO2) was followed for isolation. The pellet was dried and stored at room temperature. ICP-MS samples were prepared by digestion using 70% nitric acid (100 μ L for the mitochondria, 600 μ L for nuclei, 60 °C overnight). Samples were then further diluted 1:300 for nuclei and 1:100 for mitochondria (2% HCl solution in MQ water). Finally, the ruthenium concentration in the solution was analysed using a high resolution ICP-MS of Agilent 7900 quadrupole ICP-MS instrument at the Institut de Physique du Globe de Paris, France. To calculate the relative amount of metal present in the mitochondria, 10% of total cells suspension was taken

out from each replicate before fractionation. Then, the amount of metal present in the total cells was compared to the metal in the isolated mitochondria fraction by normalizing by the initial cell number.

Mito Stress Test

1×10^4 CT26 cells/well were seeded in a Seahorse XF Cell 96 wells Culture Microplate using 80 μ L of F12K medium supplemented with 10% FBS and incubated for 24 h at 37°C with 5% CO₂. The day after, the medium was replaced by equal volume of compound dissolved in culture media (Compound **1**, IC₂₅ = 0.025 μ M, IC₅₀ = 0.09 μ M; Compound **4**, IC₂₅ = 0.06 μ M, IC₅₀ = 0.02 μ M and PpIX, IC₂₅ = 0.004 μ M, IC₅₀ = 0.01 μ M). After 4 h of treatment, media was removed, and the treated cells were washed very carefully with the Seahorse XF medium three times. Cells were irradiated for 40 min at 540 nm. Finally, the plates were incubated at 37°C for 1 h in a non-CO₂ incubator. The Mito Stress assay was run in an Agilent Seahorse XFe96 instrument, at 37°C using multiple inhibitors, i.e., ATP synthase inhibitor (oligomycin, 1 μ M), proton gradient and mitochondrial membrane potential collapsing agent (FCCP, 1 μ M), mitochondrial respiratory complex I and III inhibitor (rotenone, 1 μ M and antimycin A, 1 μ M respectively). At the end of the run, the cells were fixed using 4% *p*-formaldehyde solution and stained with Hoechst 33342. Each well was imaged in Cytation 5 Cell Imaging Multimode Reader, BioTek using a 10X objective lens. Finally, the number of cells from each image was calculated by using Gen5 software and by utilising the cell count and the data was normalised against the same cell number.

Synthetic Procedures



Ru(DMSO)₄Cl₂ was synthesized following an adapted literature procedure.⁵⁷ Spectroscopic data were in agreement with the literature.⁵⁷

¹H NMR (400 MHz, Deuterium Oxide) δ 3.48 (s, 1H), 3.48 (s, 2H), 3.45 (s, 2H), 3.41 (s, 1H), 3.37 (s, 3H).



This precursor was synthesized according to literature procedure. Ru(DIP)₂Cl₂ was synthesized following an adapted literature procedure.⁵⁸ Spectroscopic data were in agreement with the literature.⁵⁸

¹H NMR (400 MHz, CH₃CN-*d*₃) δ 10.51 (d, *J* = 5.3 Hz, 2H), 8.17 (d, *J* = 9.4 Hz, 2H), 8.08 (d, *J* = 5.4 Hz, 2H), 8.02 (d, *J* = 9.4 Hz, 4H), 7.81 (d, *J* = 7.4 Hz, 5H), 7.70 (t, *J* = 7.4 Hz, 5H), 7.67 – 7.58 (m, 4H), 7.52 (d, *J* = 1.8 Hz, 12H), 7.25 (d, *J* = 5.5 Hz, 2H).

[Ru(DIP)₂(phen)]Cl₂

This compound was synthesized according to literature procedure. Ru(DIP)₂Cl₂ was synthesized following an adapted literature procedure.⁵⁹ Spectroscopic data were in agreement with the literature.⁵⁹ (385 mg, 73%)

Crystal Data for C₆₀H₄₀Cl₂N₆O₃Ru (*M* = 1064.95 g/mol): orthorhombic, space group Pcca (no. 54), *a* = 20.2027(4) Å, *b* = 22.3997(6) Å, *c* = 21.7393(4) Å, *V* = 9837.8(4) Å³, *Z* = 8, *T* = 100 K, μ(CuKα) = 4.013 mm⁻¹, *D*_{calc} = 1.438 g/cm³, 60181 reflections measured (7.16° ≤ 2θ ≤ 152.84°), 10029 unique (*R*_{int} = 0.0796, *R*_{sigma} = 0.0502) which were used in all calculations. The final *R*₁ was 0.0703 (*I* > 2σ(*I*)) and *wR*₂ was 0.2196 (all data). The coordinates have been deposited in the Cambridge Crystallographic Data Centre, no 2287795. ¹H NMR (400 MHz, DMSO-*d*₆) δ 8.84 (dd, *J* = 8.3, 1.2 Hz, 2H), 8.44 (s, 2H), 8.35 (d, *J* = 5.5 Hz, 2H), 8.26 (s, 4H), 8.25 (d, *J* = 1.3 Hz, 2H), 8.19 (d, *J* = 5.5 Hz, 2H), 7.88 (dd, *J* = 8.2, 5.3 Hz, 2H), 7.82 (d, *J* = 5.5 Hz, 2H), 7.76 (d, *J* = 5.5 Hz, 2H), 7.69 – 7.60 (m, 20H). ¹³C NMR (101 MHz, CH₃CN -*d*₃) δ 153.96, 153.52, 153.38, 149.96, 149.93, 149.54, 149.43, 148.82, 137.82, 136.66, 132.01, 130.77, 130.73, 130.55, 130.04, 129.87, 129.06, 127.00, 126.94. HRMS (ESI) *m/z*: [M]²⁺ Calcd for C₆₀H₄₀N₆Ru 473.1174. Found 473.1161; (Error: 0.2 ppm) IR (neat) ν max: 3053, 1621, 1556, 1415, 848 cm⁻¹. Anal. Calcd. For C₆₀H₅₀Cl₂N₆O₅Ru·5H₂O: C 65.10, H 4.55, N 7.59. Found: C 64.71, H 4.28, N 7.51. HPLC: *T*_R = 15.791 min.

1,4,5,8-tetraazaphenanthrene (TAP)

The TAP ligand was synthesized by the procedure reported in the literature.⁶⁰ Spectroscopic data were in agreement with the literature.⁶⁰

¹H NMR (400 MHz, DMSO-*d*₆) δ 9.23 (d, *J* = 2.0 Hz, 1H), 9.20 (d, *J* = 2.0 Hz, 1H), 8.37 (s, 1H). ¹³C NMR (101 MHz, DMSO-*d*₆) δ 147.36, 146.14, 143.95, 140.68, 132.00.

[Ru(DIP)₂(TAP)]Cl₂

Ru(DIP)₂Cl₂ (200 mg, 0.2 mmol) and 1,4,5,8-tetraazaphenanthrene (43.5 mg, 0.2 mmol, 1 equiv) were dissolved in DMF (20 mL) and stirred reflux for 8 h under N₂ atmosphere. The solvent was then removed *in vacuum*. The residue was purified by silica gel column chromatography (CHCl₃:CH₃OH = 3:1) to obtain an orange powder (104 mg, 42%).

¹H NMR (500 MHz, CH₃CN-*d*₃) δ 9.01 (d, *J* = 2.8 Hz, 1H, H_b), 8.63 (s, 1H, H_c), 8.41 (d, *J* = 2.8 Hz, 1H, H_a), 8.27 (d, *J* = 5.5 Hz, 1H, H₁), 8.23 (d, *J* = 5.5 Hz, 1H, H₆), 8.22 (d, *J* = 0.9 Hz, 2H, H_{3,4}), 7.70 (d, *J* = 5.5 Hz, 1H, H₂), 7.68 – 7.58 (m, 11H). ¹³C NMR (126 MHz, CH₃CN-*d*₃) δ 154.26, 153.49, 150.96, 150.29, 149.61, 149.01, 148.96, 146.46, 144.17, 136.56, 136.53, 133.77, 130.80, 130.75, 130.15, 130.10, 127.15, 127.08. HRMS (ESI) *m/z*: [M+H]⁺ Calcd for C₆₀H₄₄N₈RuH 979.2805. Found 979.2765; [M]²⁺ Found 474.11. IR (neat) ν max: 3053, 1660, 1621, 1557, 1416, 859 cm⁻¹. Anal. Calcd. For C₅₈H₅₂Cl₂F₁₂N₈O₇Ru·7H₂O: C 60.84, H 4.58, N 9.79. Found: C 60.78, H 4.21, N 9.84. HPLC: T_R = 11.302 min.

[RuCl₂(phendione)₂]

The product was synthesized following a reported protocol.⁵² Spectroscopic data were in agreement with the literature.⁵²

¹H NMR (400 MHz, DMSO-*d*₆) δ 10.11 (d, *J* = 5.2 Hz, 1H), 8.48 (d, *J* = 7.6 Hz, 1H), 8.10 (d, *J* = 7.6 Hz, 1H), 8.07 – 7.97 (m, 1H), 7.77 (d, *J* = 5.3 Hz, 1H), 7.43 – 7.27 (m, 1H).

[Ru(phendione)₂(phen)](PF₆)₂

The product was synthesized following a literature procedure.⁶¹

¹H NMR (400 MHz, DMSO-*d*₆) δ 10.12 (d, *J* = 5.7 Hz, 2H), 8.48 (d, *J* = 7.3 Hz, 2H), 8.10 (d, *J* = 7.9 Hz, 2H), 8.06 – 7.96 (m, 2H), 7.77 (d, *J* = 4.9 Hz, 2H), 7.41 – 7.29 (m, 2H). ¹³C NMR (101 MHz, CH₃CN-*d*₃) δ 208.87 (d, *J* = 31.1 Hz), 176.00 (d, *J* = 54.4 Hz), 158.02, 157.31, 154.20, 148.40, 138.81, 137.55, 137.31, 132.33, 131.84, 129.79, 129.26, 127.13.

[Ru(dppz)₂phen](PF₆)₂

[Ru(phendione)₂phen](PF₆)₂ (90 mg, 0.09 mmol) and *o*-phenylenediamine (40 mg, 0.36 mmol, 4 equiv.) were added to a mixture of degassed CH₃CN:EtOH (20 mL, 1:3, v/v) and stirred at 80°C for 20 h under N₂ atmosphere. The reaction mixture was concentrated to ca. 10 mL and cooled to room temperature, then an aqueous saturated NH₄PF₆ solution (15 mL) was added. A red precipitate was formed, and the mixture was kept at 4°C overnight to allow the complete precipitation. The red product was collected by vacuum filtration, washed with distilled water, ice cold ethanol, and dried

with diethyl ether. The product was then redissolved in CH₃CN and dried *in vacuo*. (Aspect: red powder, 88 mg, 82%). The PF₆⁻ counterion was exchanged by using Amberlite® IRA402 chloride form resin. The compound was dissolved in 1 mL of MeCN and 5 mL of MeOH was added. The resin was added and mixed by rotation for 5 hours. After cotton filtration the compound was precipitated in pentane to remove grease traces from the resin and dried under vacuum.

Crystal Data for C₁₉₂H₁₁₂F₄₈N₄₀P₈Ru₄ (*M* = 4542.24 g/mol): monoclinic, space group P2₁/n (no. 14), *a* = 21.8071(12) Å, *b* = 30.1739(17) Å, *c* = 28.475(2) Å, *β* = 103.157(7)°, *V* = 18245(2) Å³, *Z* = 4, *T* = 293(2) K, *μ*(MoKα) = 0.512 mm⁻¹, *D*_{calc} = 1.654 g/cm³, 603650 reflections measured (3.99° ≤ 2θ ≤ 46.514°), 26192 unique (*R*_{int} = 0.4362, *R*_{sigma} = 0.0989) which were used in all calculations. The final *R*₁ was 0.1178 (*I* > 2σ(*I*)) and *wR*₂ was 0.3693 (all data). The coordinates have been deposited in the Cambridge Crystallographic Data Centre (CCDC), deposition number no. 2277028. ¹H NMR (400 MHz, CH₃CN-*d*₃) δ 9.67 (ddd, *J* = 8.3, 5.4, 1.3 Hz, 4H, H_{3 or 4}), 8.65 (dd, *J* = 8.3, 1.3 Hz, 2H, H_c), 8.52 – 8.46 (m, 4H, H_{7 or 10}), 8.31 (dd, *J* = 5.4, 1.3 Hz, 2H, H₁), 8.29 (s, 2H, H_d), 8.22 (dd, *J* = 5.3, 1.2 Hz, 2H, H_a), 8.17 – 8.13 (m, 4H, H_{8 or 9}), 8.11 (dd, *J* = 5.4, 1.3 Hz, 2H, H₆), 7.83 (dd, *J* = 8.2, 5.4 Hz, 2H, H₂), 7.81 (ddd, *J* = 12.8, 8.3, 5.4 Hz, 4H, H₅), 7.68 (dd, *J* = 8.3, 5.3 Hz, 2H, H_b). ¹³C NMR (101 MHz, CH₃CN-*d*₃) δ 155.46, 155.21, 154.23, 151.85, 151.77, 148.78, 143.79, 141.06, 138.13, 134.66, 134.61, 133.56, 132.14, 131.88, 130.65, 129.14, 128.31, 128.25, 126.98. HRMS (ESI) *m/z*: [M]²⁺ Calcd for C₄₈H₂₈N₁₀Ru 423.07. Found 423.07. IR (neat) *v* max: 3097, 1617, 1546, 1421, 1358, 843 cm⁻¹. HPLC: *T*_R = 10.734 min.

[Ru(*dppn*)₂phen](PF₆)₂

[Ru(phenadione)₂phen](PF₆)₂ (113 mg, 0.11 mmol, 1 equiv.) and 2,3-diaminonaphtalene (72 mg, 0.46 mmol, 4 equiv.) were suspended in degassed CH₃CN:EtOH (25 mL, 1:3, v/v) and stirred at 80 °C for 20 h under N₂ atmosphere. The reaction mixture was concentrated *in vacuo* to ca. 10 mL and cooled to room temperature, followed by the addition of an aqueous saturated NH₄PF₆ solution (15 mL). The formation of a dark red precipitate was observed. The mixture was kept at 4°C overnight to allow the complete precipitation. The brown product was collected by vacuum filtration, washed with distilled water, ice cold ethanol, and dried with diethyl ether. The product redissolved in acetonitrile and dried *in vacuo*. (Aspect: dark red powder, 106 mg, 55%).

¹H NMR (400 MHz, CH₃CN-*d*₃) δ 9.68 (ddd, *J* = 9.5, 8.2, 1.4 Hz, 2H, H_{3 or 6}), 9.15 (s, 2H, H_{7 or 12}), 8.66 (dd, *J* = 8.3, 1.3 Hz, 1H, H_c), 8.42 – 8.35 (m, 2H, H_{8 or 11}), 8.33 (dd, *J* = 5.4, 1.3 Hz, 1H, H_{1 or 4}), 8.30 (s,

¹H, H_d), 8.27 (dd, *J* = 5.3, 1.3 Hz, 1H, H_a), 8.08 (dd, *J* = 5.4, 1.3 Hz, 1H, H_{1 or 4}), 7.84 (dd, *J* = 8.2, 5.5 Hz, 1H, H_{2 or 5}), 7.81 – 7.74 (m, 3H, H_{9 or 10}), 7.71 (dd, *J* = 8.3, 5.3 Hz, 1H, H_b). ¹³C NMR (126 MHz, CH₃CN-*d*₃) δ 155.56, 155.26, 154.29, 152.49, 152.40, 148.78, 141.94, 139.73, 138.19, 136.27, 134.79, 134.72, 132.26, 132.18, 129.64, 129.34, 129.16, 128.50, 128.46, 127.03. HRMS (ESI) *m/z*: [M]²⁺ Calcd for C₆₀H₄₀N₆Ru 473.0922. Found 473.0926; (Error: 0.2 ppm) IR (neat) *v* max: 3088, 1632, 1515, 1419, 1357, 842 cm⁻¹. Anal. Calcd. For C₅₆H₃₂F₁₂N₁₀P₂Ru·4H₂O: C 51.42, H 3.08, N 10.71. Found: C 51.18, H 2.88, N 10.16. HPLC: T_R = 11.689 min.

Acknowledgments

We are grateful for financial support from the European Union's Horizon 2020 research and innovation programme (Marie Skłodowska-Curie grant agreement No. 861381), the ERC Consolidator Grant PhotoMedMet to G.G. (GA 681679), the program "Investissements d' Avenir" launched by the French Government and implemented by the ANR with the reference ANR-10-IDEX-0001-02 PSL (G.G.). This work was carried out with the support of Diamond Light Source, instrument B23 (proposal number SM30390). Part of the ICP-MS analyses were supported by IPGP multidisciplinary program PARI, and by Paris-IdF region SESAME Grant no. 12015908.

Supporting Information

¹H, ¹³C NMR spectra, HPLC chromatogram, HRMS (Figure SI1-SI16). Crystal Data collection and refinements (Table SI1, SI2). Structure of the compounds with protons enumeration (Figure SI17). Crystal data collection and results (Table SI1-2). Crystal structure showing π-π stacking interactions between the ligands (Figure SI18-19). Luminescence spectra (Figure SI20). Luminescence decays (Figure SI21, Table SI3). Luminescence lifetime (Table SI3). Singlet oxygen emission spectra (Figure SI22). Photobleaching studies by UV (Figure SI23). Stability studies by ¹H NMR in DMSO of compounds **1-4** at 37°C (Figure SI24-SI27). IC₅₀ plots of the compounds at different wavelengths (SI28-SI39). Cellular uptake graphs (Figure SI40). CD melting profile of (CCGGCGCCGG)₂ and d(CCGGTACCGG)₂ with **3** (1:0, 1:1 and 1:3 ratio) (Fig. SI41-SI46).

References

- (1) Love, R.; Leventhal, H.; Easterling, D.; Nerenz, D. Side Effects and Emotional Distress During Cancer Chemotherapy. *Cancer Chemother. Pharmacol.* **1989**, 604–612.

- (2) Correia, J. H.; Rodrigues, J. A.; Pimenta, S.; Dong, T.; Yang, Z. Photodynamic Therapy Review: Principles, Photosensitizers, Applications, and Future Directions. *Pharmaceutics* **2021**, *13* (9), 1–16. <https://doi.org/10.3390/pharmaceutics13091332>.
- (3) Gunaydin, G.; Gedik, M. E.; Ayan, S. Photodynamic Therapy for the Treatment and Diagnosis of Cancer—A Review of the Current Clinical Status. *Front. Chem.* **2021**, *9* (August), 1–26. <https://doi.org/10.3389/fchem.2021.686303>.
- (4) Wang, L.; Yin, H.; Javed, M. A.; Hetu, M.; Wang, C.; Monroe, S.; Zhu, X.; Kilina, S.; McFarland, S. A.; Sun, W. π -Expansive Heteroleptic Ruthenium(II) Complexes as Reverse Saturable Absorbers and Photosensitizers for Photodynamic Therapy. *Inorg. Chem.* **2017**, *56*, 3245–3259. <https://doi.org/10.1021/acs.inorgchem.6b02624>.
- (5) Ghosh, G.; Colo, K. L.; Fuller, A.; Sainuddin, T.; Bradner, E.; McCain, J.; Monroe, S. M. A.; Yin, H.; Hetu, M. W.; Cameron, C. G.; McFarland, S. A. Cyclometalated Ruthenium(II) Complexes Derived from α -Oligothiophenes as Highly Selective Cytotoxic or Photocytotoxic Agents. *Inorg. Chem.* **2018**, *57*, 7694–7712. <https://doi.org/10.1021/acs.inorgchem.8b00689>.
- (6) Liu, J.; Chen, Y.; Li, G.; Zhang, P.; Jin, C.; Zeng, L.; Ji, L.; Chao, H. Ruthenium(II) Polypyridyl Complexes as Mitochondria-Targeted Two-Photon Photodynamic Anticancer Agents. *Biomaterials* **2015**, *56*, 140–153. <https://doi.org/10.1016/j.biomaterials.2015.04.002>.
- (7) Li, G.; Sun, L.; Ji, L.; Chao, H. Ruthenium(II) Complexes with Dppz: From Molecular Photoswitch to Biological Applications. *Dalt. Trans.* **2016**, *45* (34), 13261–13276. <https://doi.org/10.1039/c6dt01624c>.
- (8) Tang, S.; Wang, M.; Yang, R.; Liu, M.; Li, Q.; Gao, F. More-Is-Better Strategy for Constructing Homoligand Polypyridyl Ruthenium Complexes as Photosensitizers for Infrared Two-Photon Photodynamic Therapy. *Inorg. Chem.* **2023**, *62* (21), 8210–8218. <https://doi.org/10.1021/acs.inorgchem.3c00585>.
- (9) Wachter, E.; Heidary, D. K.; Howerton, B. S.; Parkin, S.; Glazer, E. C. Light-Activated Ruthenium Complexes Photobind DNA and Are Cytotoxic in the Photodynamic Therapy Window. *Chem. Commun* **2012**, *48*, 9649–9651. <https://doi.org/10.1039/c2cc33359g>.
- (10) Karges, J.; Kuang, S.; Maschietto, F.; Blacque, O.; Ciofini, I.; Chao, H.; Gasser, G. Rationally Designed Ruthenium Complexes for 1- and 2-Photon Photodynamic Therapy. *Nat. Commun.* **2020**, *11* (1), 1–13. <https://doi.org/10.1038/s41467-020-16993-0>.

- (11) Karges, J.; Heinemann, F.; Jakubaszek, M.; Maschietto, F.; Subecz, C.; Dotou, M.; Vinck, R.; Blacque, O.; Tharaud, M.; Goud, B.; Viñuelas Zahlnos, E.; Spingler, B.; Ciofini, I.; Gasser, G. Rationally Designed Long-Wavelength Absorbing Ru(II) Polypyridyl Complexes as Photosensitizers for Photodynamic Therapy. *J. Am. Chem. Soc.* **2020**, *142* (14), 6578–6587. <https://doi.org/10.1021/jacs.9b13620>.
- (12) Heinemann, F.; Karges, J.; Gasser, G. Critical Overview of the Use of Ru(II) Polypyridyl Complexes as Photosensitizers in One-Photon and Two-Photon Photodynamic Therapy. *Acc. Chem. Res.* **2017**, *50*, 2727–2736. <https://doi.org/10.1021/acs.accounts.7b00180>.
- (13) Mari, C.; Pierroz, V.; Rubbiani, R.; Patra, M.; Hess, J.; Spingler, B.; Oehninger, L.; Schur, J.; Ott, I.; Salassa, L.; Ferrari, S.; Gasser, G. DNA Intercalating Ru(II) Polypyridyl Complexes as Effective Photosensitizers in Photodynamic Therapy. *Chem. - A Eur. J.* **2014**, *20* (44), 14421–14436. <https://doi.org/10.1002/chem.201402796>.
- (14) Gandioso, A.; Purkait, K.; Gasser, G. Recent Approaches towards the Development of Ru(II) Polypyridyl Complexes for Anticancer Photodynamic Therapy. *Chimia (Aarau)*. **2021**, *75* (10), 845–855. <https://doi.org/10.2533/chimia.2021.845>.
- (15) Chamberlain, S.; Cole, H. D.; Roque, J.; Bellnier, D.; McFarland, S. A.; Shafirstein, G. Tld1433-Mediated Photodynamic Therapy with an Optical Surface Applicator in the Treatment of Lung Cancer Cells in Vitro. *Pharmaceuticals* **2020**, *13* (7), 1–9. <https://doi.org/10.3390/ph13070137>.
- (16) Monro, S.; Colón, K. L.; Yin, H.; III, J. R.; Konda, P.; Gujar, S.; Thummel, R. P.; Lilge, L.; Colin G. Cameron, and S. A. M. Transition Metal Complexes and Photodynamic Therapy from a Tumor-Centered Approach: Challenges, Opportunities, and Highlights from the Development of TLD1433. *Chem. Rev.* **2019**, *119* (2), 797–828. <https://doi.org/10.1021/acs.chemrev.8b00211>.Transition.
- (17) Toupin, N. P.; Nadella, S.; Steinke, S. J.; Turro, C.; Kodanko, J. J. Dual-Action Ru(II) Complexes with Bulky π -Expansive Ligands: Phototoxicity without DNA Intercalation. *Inorg. Chem.* **2020**, *59*, 3919–3933. <https://doi.org/10.1021/acs.inorgchem.9b03585>.
- (18) Friedman, A. E.; Chambron, J.; Sauvage, J.; Turro, N. J.; Barton, J. K. Molecular “Light Switch” for DNA: Ru(Bpy)₂(Dppz)₂⁺. *J. Am. Chem. Soc.* **1990**, *112* (11), 4960–4962.
- (19) Hartshorn, R. M.; Barton, J. K. Novel Dipyridophenazine Complexes of Ruthenium(II):

Exploring Luminescent Reporters of DNA. *J. Am. Chem. Soc.* **1992**, *114* (15), 5919–5925.
<https://doi.org/10.1021/ja00041a002>.

- (20) Schatzschneider, U.; Nielsen, J.; Ott, I.; Gust, R.; Alborzina, H.; Wolf, S. Cellular Uptake , Cytotoxicity , and Metabolic Profiling of Human Cancer Cells Treated with Ruthenium(II) Polypyridyl Complexes [Ru(Bpy)₂(N-N)]Cl₂ with N-N=bpy, Phen, Dpq, Dppz, and Dppn. *chem med chem* **2008**, *3*, 1104–1109. <https://doi.org/10.1002/cmdc.200800039>.
- (21) Komor, A. C.; Barton, J. K. The Path for Metal Complexes to a DNA Target. *Chem. Commun* **2013**, *49*, 3617–3630. <https://doi.org/10.1039/c3cc00177f>.
- (22) Wu, Z.; Tian, T.; Yu, J.; Weng, X.; Liu, Y.; Zhou, X. Formation of Sequence-Independent Z-DNA Induced by a Ruthenium Complex at Low Salt Concentrations. *Angew. Chemie - Int. Ed.* **2011**, *50* (50), 11962–11967. <https://doi.org/10.1002/anie.201104422>.
- (23) Albano, G.; Belser, P.; Daul, C. π^* Level Tuning in a Series of Diimine Ligands Based on Density Functional Theory: Application to Photonic Devices. *Inorg. Chem.* **2001**, *40* (7), 1408–1413. <https://doi.org/10.1021/ic000694c>.
- (24) Giacomazzo, G. E.; Schlich, M.; Casula, L.; Galantini, L.; Giudice, A. Del; Pietraperzia, G.; Sinico, C.; Cencetti, F.; Pecchioli, S.; Valtancoli, B.; Conti, L.; Murgia, S.; Giorgi, C. Ruthenium(II) Polypyridyl Complexes with π -Expansive Ligands: Synthesis and Cubosome Encapsulation for Photodynamic Therapy of Non-Melanoma Skin Cancer. *Inorg. Chem. Front.* **2023**, *6* (1). <https://doi.org/10.1039/D2QI02678C>.
- (25) Leveque, J.; Elias, B.; Moucheron, C.; Kirsch-De Mesmaeker, A. Dendritic Tetranuclear Ru(II) Complexes Based on the Nonsymmetrical PHEHAT Bridging Ligand and Their Building Blocks: Synthesis, Characterization, and Electrochemical and Photophysical Properties. *Inorg. Chem.* **2005**, *44* (2), 393–400. <https://doi.org/10.1021/ic048941q>.
- (26) Evans, I. P.; Spencer, A.; Wilkinson G. Dichlorotetrakis(Dimethyl Sulphoxide)Ruthenium(II) and Its Use as a Source Material for Some New Ruthenium(II) Complexes. *Chem. Lett.* **1971**, *7* (781), 204–209.
- (27) Sun, J.; Wu, S.; An, Y.; Liu, J.; Gao, F.; Ji, L. N.; Mao, Z. W. Synthesis, Crystal Structure and DNA-Binding Properties of Ruthenium(II) Polypyridyl Complexes with Dicationic 2,2' - Dipyridyl Derivatives as Ligands. *Polyhedron* **2008**, *27* (13), 2845–2850. <https://doi.org/10.1016/j.poly.2008.06.009>.

- (28) Finlayson, L.; Barnard, I. R. M.; McMillan, L.; Ibbotson, S. H.; Brown, C. T. A.; Eadie, E.; Wood, K. Depth Penetration of Light into Skin as a Function of Wavelength from 200 to 1000 Nm. *Photochem. Photobiol.* **2022**, *98* (4), 974–981. <https://doi.org/10.1111/php.13550>.
- (29) Martinez-Alonso, M.; Gandioso, A.; Thibaudeau, C.; Qin, X.; Arnoux, P.; Demeubayeva, N.; Guérineau, V.; Frochot, C.; Jung, A. C.; Gaiddon, C.; Gasser, G. A Novel Near-IR Absorbing Ruthenium(II) Complex as Photosensitizer for Photodynamic Therapy and Its Cetuximab Bioconjugat. *ChemBioChem* **2023**, *24*. <https://doi.org/10.1002/cbic.202300203>.
- (30) Liu, X.; Testa, B.; Fahr, A. Lipophilicity and Its Relationship with Passive Drug Permeation. *Pharm Res* **2011**, *28*, 962–977. <https://doi.org/10.1007/s11095-010-0303-7>.
- (31) Poole, S. K.; Poole, C. F. Separation Methods for Estimating Octanol – Water Partition Coefficients. *J. Chromatogr.* **2003**, *797*, 3–19. <https://doi.org/10.1016/j.jchromb.2003.08.032>.
- (32) Bonnett, R.; Martõ, G. Photobleaching of Sensitisers Used in Photodynamic Therapy. *tetrahedron* **2001**, *57* (591), 9513–9543.
- (33) Mani, A.; Feng, T.; Gandioso, A.; Vinck, R.; Notaro, A.; Gourdon, L.; Burckel, P.; Saubaméa, B.; Blacque, O.; Cariou, K.; Belgaied, J. E.; Chao, H.; Gasser, G. Structurally Simple Osmium(II) Polypyridyl Complexes as Photosensitizers for Photodynamic Therapy in the Near Infrared**. *Angew. Chemie* **2023**, *62* (20). <https://doi.org/10.1002/anie.202218347>.
- (34) Zhang, L.; Wang, P.; Zhou, X.-Q.; Bretin, L.; Zeng, X.; Husiev, Y.; Polanco, E. A.; Zhao, G.; Wijaya, L. S.; Biver, T.; Le Dévédec, S. E.; Sun, W.; Bonnet, S. Cyclic Ruthenium-Peptide Conjugates as Integrin-Targeting Phototherapeutic Prodrugs for the Treatment of Brain Tumors. *J. Am. Chem. Soc.* **2023**, *145*, 1496–14980. <https://doi.org/10.1021/jacs.3c04855>.
- (35) Pervaiz, S.; Malini, O. Art and Science of Photodynamic Therapy. *Clin. Exp. Pharmacol. Physiol.* **2006**, *33*, 551–556.
- (36) Cardin, C. J.; Kelly, J. M.; Quinn, S. J. Photochemically Active DNA-Intercalating Ruthenium and Related Complexes-Insights by Combining Crystallography and Transient Spectroscopy. *Chem. Sci.* **2017**, *8* (7), 4705–4723. <https://doi.org/10.1039/c7sc01070b>.
- (37) Jia, F.; Wang, S.; Man, Y.; Kumar, P.; Liu, B. Recent Developments in the Interactions of Classic. **2019**, No. Figure 1. <https://doi.org/10.3390/molecules24040769>.
- (38) Hall, J. P.; Sullivan, K. O.; Naseer, A.; Smith, J. A.; Kelly, J. M.; Cardin, C. J. Structure

Determination of an Intercalating Ruthenium Dipyridophenazine Complex Which Kinks DNA by Semiintercalation of a Tetraazaphenanthrene Ligand. *PNAS* **2011**, *108* (17610–17614), 2–6. <https://doi.org/10.1073/pnas.1108685108>.

- (39) Niyazi, H.; Hall, J. P.; Sullivan, K. O.; Winter, G.; Sorensen, T.; Kelly, J. M.; Cardin, C. J. Crystal Structures of L-[Ru(Phen)₂dppz]²⁺ with Oligonucleotides Containing TA/TA and AT/AT Steps Show Two Intercalation Modes. *Nat. Chem.* **2012**, *4*, 621–628. <https://doi.org/10.1038/nchem.1397>.
- (40) Li, W.; Liu, X.; Tan, L. Binding Properties of [Ru(Phen)₂(11-R-Dppz)]²⁺ (R=F or CN) with Poly (A)•poly (U) Duplex RNA. *J. Inorg. Biochem.* **2022**, *232* (111833), 1–4. <https://doi.org/10.1016/j.jinorgbio.2022.111833>.
- (41) Kulms, D.; Schwarz, T. Molecular Mechanisms of UV-Induced Apoptosis. *Photodermatol. Photoimmunol. Photomed.* **2000**, *16* (7), 195–201.
- (42) Sakhrani, N. M.; Padh, H. Organelle Targeting: Third Level of Drug Targeting. *Drug Des. Devel. Ther.* **2013**, *7*, 585–599. <https://doi.org/10.2147/DDDT.S45614>.
- (43) Hockenbery, D. M. Targeting Mitochondria for Cancer Therapy. *Environ. Mol. Mutagen.* **2010**, *51*, 476–489. <https://doi.org/doi:10.1002/em.20552>.
- (44) Qian, C.; Wang, J. Q.; Song, C. L.; Wang, L. L.; Ji, L. N.; Chao, H. The Induction of Mitochondria-Mediated Apoptosis in Cancer Cells by Ruthenium(II) Asymmetric Complexes. *Metallomics* **2013**, *5* (7), 844–854. <https://doi.org/10.1039/c3mt20270d>.
- (45) Brand, M. D.; Orr A. L., P. I. V.; Quinlan C. L. The Role of Mitochondrial Function and Cellular Bioenergetics in Ageing and Disease. *Br J. Dermatol.* **2013**, *23* (1), 1–19. <https://doi.org/10.1111/bjd.12208>.The.
- (46) Osellame, L. D.; Blacker, T. S.; Duchon, M. R. Cellular and Molecular Mechanisms of Mitochondrial Function. *Best Pract. Res. Clin. Endocrinol. Metab.* **2012**, *26* (6), 711–723. <https://doi.org/10.1016/j.beem.2012.05.003>.
- (47) Wallace, D. C. Mitochondria and Cancer. *Nat. Rev. Cancer* **2012**, *12* (10), 685–698. <https://doi.org/10.1038/nrc3365>.
- (48) Agilent Technologies. *Mito Stress Test Kit User Guide*; 2019.
- (49) Zeng, C. C.; Jiang, G. Bin; Lai, S. H.; Zhang, C.; Yin, H.; Tang, B.; Wan, D.; Liu, Y. J. Synthesis,

Characterization and Anticancer Activity Studies of Ruthenium(II) Polypyridyl Complexes on A549 Cells. *J. Photochem. Photobiol. B Biol.* **2016**, *161*, 295–303.

<https://doi.org/10.1016/j.jphotobiol.2016.06.004>.

- (50) Lin, G. J.; Jiang, G. Bin; Xie, Y. Y.; Huang, H. L.; Liang, Z. H.; Liu, Y. J. Cytotoxicity, Apoptosis, Cell Cycle Arrest, Reactive Oxygen Species, Mitochondrial Membrane Potential, and Western Blotting Analysis of Ruthenium(II) Complexes. *J. Biol. Inorg. Chem.* **2013**, *18* (8), 873–882. <https://doi.org/10.1007/s00775-013-1032-2>.
- (51) Dip, R.; Otf, M.; Caspar, R.; Cordier, C.; Waern, J. B.; Guyard-duhayon, C.; Gruselle, M. A New Family of Mono- and Dicarboxylic Ruthenium Complexes. **2006**, *45* (10), 58–62.
- (52) Pinczewska, A.; Sosna, M.; Bloodworth, S.; Kilburn, J. D.; Bartlett, P. N. High-Throughput Synthesis and Electrochemical Screening of a Library of Modified Electrodes for NADH Oxidation. *J. Am. Chem. Soc.* **2012**, *134*, 18022–18033.
- (53) Dolomanov, O. V.; Bourhis, L. J.; Gildea, R. J.; Howard, J. A. K.; Puschmann, H. OLEX2: A Complete Structure Solution, Refinement and Analysis Program. *J. Appl. Crystallogr.* **2009**, *42* (2), 339–341. <https://doi.org/10.1107/S0021889808042726>.
- (54) Sheldrick, G. M. Crystal Structure Refinement with SHELXL. *Acta Crystallogr. Sect.* **2015**, *71*, 3–8. <https://doi.org/10.1107/S2053229614024218>.
- (55) Ishida, H.; Tobita, S.; Hasegawa, Y.; Katoh, R.; Nozaki, K. Recent Advances in Instrumentation for Absolute Emission Quantum Yield Measurements. *Coord. Chem. Rev.* **2010**, *254* (21–22), 2449–2458. <https://doi.org/10.1016/j.ccr.2010.04.006>.
- (56) Ghosh, H. Yin, S.M.A. Monro, T. Sainuddin, L. Lapoot, A. Greer, S.A. McFarland, *Photochem. Photobiol.* **2020**, *96*, 349-357. <https://doi.org/10.1111/php.13177>.
- (57) Alessio, E. Synthesis and Reactivity of Ru-, Os-, Rh-, and Ir-Halide – Sulfoxide Complexes. *Chem. Rev.* **2004**, *104*, 4203–4242.
- (58) Munteanu, A.; Notaro, A.; Jakubaszek, M.; Cowell, J.; Goud, B.; Uivarosi, V.; Gasser, G. Synthesis, Characterization, Cytotoxic Activity, and Metabolic Studies of Ruthenium(II) Polypyridyl Complexes Containing Flavonoid Ligands. *Inorg.* **2019**. <https://doi.org/10.1021/acs.inorgchem.9b03562>.
- (59) Pinczewska, A.; Sosna, M.; Bloodworth, S.; Kilburn, J. D.; Bartlett, P. N. High-Throughput Synthesis and Electrochemical Screening of a Library of Modified Electrodes for NADH

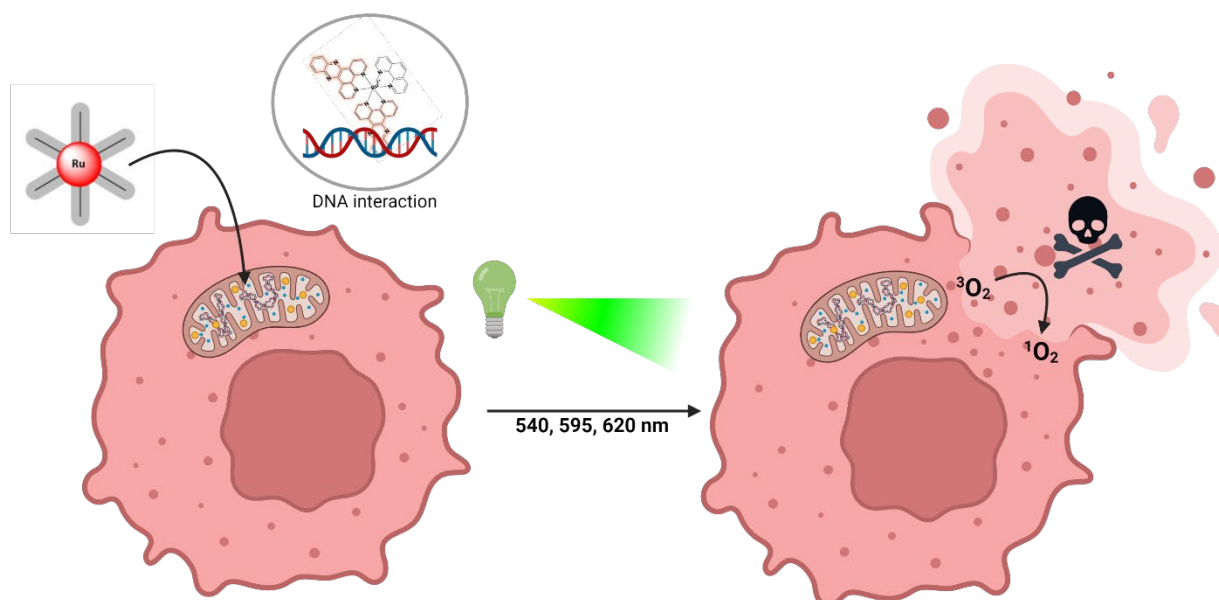
Oxidation. *J. Am. Chem. Soc* **2012**, *134*, 18022–18033. <https://doi.org/10.1021/ja307390x>.

- (60) Ortmans, I.; Elias, B.; Kelly, J. M.; Moucheron, C.; Kirsch-DeMesmaeker, A. [Ru(TAP)₂(Dppz)]²⁺: A DNA Intercalating Complex, Which Luminesces Strongly in Water and Undergoes Photo-Induced Proton-Coupled Electron Transfer with Guanosine-5′ - Monophosphate. *J. Chem. Soc. Dalt. Trans.* **2004**, *4* (4), 668–676. <https://doi.org/10.1039/b313213g>.
- (61) Roy, S.; Colombo, E.; Vinck, R.; Mari, C.; Rubbiani, R. Increased Lipophilicity of Halogenated Ruthenium (II) Polypyridyl Complexes Leads to Decreased Phototoxicity in Vitro When Used as Photosensitizers for Photodynamic Therapy. *ChemBioChem* **2020**, *21*, 2966–2973.

For Table of Contents Only

Synopsis

In this article, the promising phototoxicity of four Ru(II) polypyridyl compounds against two cancer cell lines and one non-cancerous cell line is described. Among these compounds, $[\text{Ru}(\text{dppn})_2(\text{phen})](\text{PF}_6)_2$ was found to have some photo-toxicity in the micro- or even nanomolar concentration range. Interestingly, this metal complex was found to influence cellular respiration upon light exposure, shedding light on promising phototoxicity and interactions with key biological components.



This graphical abstract was Created with BioRender.com.